
Article:
Offadini, Manuel and Ferreira, Aires Francisco (2018) Microscopic theory of spin relaxation anisotropy in graphene with proximity-induced spin-orbit coupling. Physical Review B. 245408. ISSN: 2469-9969

https://doi.org/10.1103/PhysRevB.98.245408

Microscopic theory of spin relaxation anisotropy in graphene with proximity-induced spin-orbit coupling

Manuel Offidani and Aires Ferreira
Department of Physics, University of York, York YO10 5DD, United Kingdom

(Received 23 July 2018; revised manuscript received 9 October 2018; published 10 December 2018)

We present a microscopic theory of spin dynamics in weakly disordered graphene with uniform proximity-induced spin-orbit coupling (SOC). A time-dependent perturbative treatment is employed to derive the spin Bloch equations governing the spin dynamics at high electronic density for arbitrary ratio $\lambda_{\rm SOC}/\eta$, where η is the disorder-induced quasiparticle broadening and $\lambda_{\rm SOC}$ is the largest spin-orbit energy scale. Rich scenarios are predicted, depending on a delicate competition between interface-induced Bychkov-Rashba and spin-valley interaction. In the motional narrowing regime of weak SOC ($\lambda_{\rm SOC} \ll \eta$), the anisotropy ratio of out-of-plane to in-plane spin lifetimes $\zeta = \tau_s^{\perp}/\tau_s^{\parallel}$ agrees qualitatively with a toy model of spins in a fluctuating SOC field proposed recently by Cummings and co-workers Phys. Rev. Lett. **119**, 206601 (2017). For well-resolved SOC ($\lambda_{\rm SOC} \gtrsim \eta$), the spin dynamics is characterized by fast damped oscillations with spins relaxing on the timescale of a single scattering event. In this regime, qualitatively different formulas for ζ are obtained, which can be useful to model spin transport in ultraclean van der Waals heterostructures.

DOI: 10.1103/PhysRevB.98.245408

I. INTRODUCTION

The tailored control of electronic properties in van der Waals heterostructures built from the assembly of two-dimensional (2D) crystals has provided a unique route to explore interface-induced phenomena [1–4]. Heterostructures combining graphene and semiconducting group-VI dichalcogenides [MX_2 (e.g., M = Mo, W; X = S, Se)] could enable low-power spin-logic devices harnessing the rich interplay between quantum (spin and valley) degrees of freedom in honeycomb-layered materials with strong spin-orbit coupling SOC [5]. This thrust has been fueled by the prospect of enhancing spin-orbital effects in graphene, while preserving the quintessential Dirac character of its 2D quasiparticles [6–8]. The much sought after interface-induced SOC has been recently demonstrated in graphene/transition metal dichalcogenide (TMD) bilayers [9–17], where sharp weak antilocalization features in the magnetoconductance data [11–15] and dramatic reduction of spin lifetime [16,17] hint at a massive enhancement of spin-orbit interactions in the 2D carbon layer (up to 10 meV), consistent with the predictions of model calculations and first-principles studies [10,18,19].

The modification of electronic states in graphene-based van der Waals heterostructures can be understood within a weak interlayer coupling picture, where the original Dirac (graphene) states located in the band gap of a 2D semiconductor are perturbed in two fundamental ways. First, the interfacial breaking of mirror inversion symmetry leads to the familiar Bychkov-Rashba (BR) effect [20]. The spin rotational invariance is lifted (point-group symmetry reduction $D_{6h} \to C_{6v}$), which causes the spin splitting of the Dirac states. Second, the proximity to metal atoms located beneath the graphene flake ($C_{6v} \to C_{3v}$) effectively "transfers" the sublattice-resolved SOC of the TMD substrate onto graphene (and hence spin-valley interactions). The type and strength of the effective spin-orbit interactions will ultimately depend on the number of layers and specific TMD, degree of vertical strain, and possible presence of resonant scatterers [18,21–24].

Proximity-induced SOC couples all internal degrees of freedom of 2D materials (i.e., spin, sublattice, and valley), thus enabling interesting nonequilibrium phenomena, such as anisotropic spin dynamics [25] and charge-to-spin interconversion via spin-Galvanic and spin-Hall effects [26–28]. In this work, we report a microscopic theory of spin dynamics in graphene with enhanced proximity spin-orbital effects. Our aim is to obtain a general microscopic description of spin relaxation processes beyond the motional narrowing regime of weak SOC [25]. We note that the effect of random SOC $\lambda(\mathbf{x})$ (e.g., with origin in ripples and impurities) has been extensively studied in previous works [24,29–33]. Here, instead, the focus is on systems with well-developed SOC in the band structure [$|\lambda(\mathbf{x})| \ll \lambda_{\rm SOC}$], which in principle can be realized in van der Waals heterotructures with an ultraclean interface [9–17]. The interface-induced spin-orbit interaction enters the long-wavelength continuum Hamiltonian as an additional uniform term $V_{\rm SO}$, that is (we choose natural units with $\hbar = 1 = e$)

$$H = \int d\mathbf{x}\, \Psi^{\dagger}(\mathbf{x})[\tau_z\, v\, \boldsymbol{\sigma}\cdot\mathbf{p} + V_{\rm SO} + U(\mathbf{x})]\Psi(\mathbf{x}), \qquad (1)$$

where v is the Fermi velocity of massless Dirac fermions, $\mathbf{p} = -\imath\nabla$ is the momentum operator around a valley, $V_{\rm SO}$ is the uniform spin-orbit interaction, and $U(x)$ is a disorder potential describing elastic scattering from nonmagnetic impurities. Here, τ_ς, σ_ς, and s_ς are Pauli matrices ($\varsigma = x, y, z$) and identity ($\varsigma = 0$) defined on valley, sublattice, and spin space, respectively [34]. While the strength of proximity-induced interactions for a given heterostructure is *a priori*

unknown, first-principles calculations and transport data provide a mean to estimate the various spin-orbit terms allowed by symmetry [35–39]. It can be easily shown that there are three such terms compatible with the C_{3v} point group, $V_{\rm SO} = H_{\rm KM} + H_{\rm BR} + H_{\rm sv}$, respectively, intrinsiclike SOC [40], BR interaction [20], and spin-valley coupling [37]. We note in passing that, beyond SOC, the proximity effect can mediate an orbital sublattice-staggered potential $H_\Delta = \Delta\,\tau_z\sigma_z$ [18]. This effect is believed to play a minor role in graphene/TMD bilayers (as opposed to graphene/*h*-BN [41]) and will be neglected in the following discussion [42]. The intrinsic-type SOC

$$H_{\rm KM} = \lambda_0\,\tau_0\,\sigma_z\,s_z \tag{2}$$

is invariant under the symmetry operations of the D_{6h} point group, and thus it is already present in pristine graphene (albeit extremely weak, $\lambda_0 \approx 20\ \mu$eV [43,44]). As shown by Kane and Mele (KM) [45], a sufficiently large λ_0 would drive graphene into a nontrivial topological insulating phase. However, this special type of SOC, which shares the same sublattice structure of the orbital interaction H_Δ, plays a secondary role for the spin dynamics in the high electronic density regime [42]. As anticipated above, in 2D heterostructures, the interfacial breaking of mirror inversion symmetry favors the appearance of BR-type SOC. This term (which is compatible with the C_{6v} point group) couples the electron's spin and velocity, acting as a non-Abelian gauge field [27]

$$H_{\rm BR} = \lambda\,\tau_z\,(\boldsymbol{\sigma}\times\mathbf{s})_z. \tag{3}$$

Finally, 2D crystals with sublattices occupied by different chemical species exhibit sublattice-resolved SOC (C_{3v} point group) [37,46,47]. This leads to a spin-valley coupling in the continuum limit

$$H_{\rm sv} = \lambda_{\rm sv}\,\tau_z\,\sigma_0\,s_z, \tag{4}$$

which is formally equivalent to a (valley-dependent) Zeeman interaction and, as such, it tends to "stabilize" out-of-plane spins. For this reason, the spin dynamics associated to in-plane ($\parallel$) and out-of-the-plane ($\perp$) channels in samples with sizable $\lambda_{\rm sv}$ is set by distinct timescales with $\tau_s^\perp \gg \tau_s^\parallel$. The anisotropy in the spin dynamics can be quantified by the *spin relaxation time anisotropy* (SRTA) ratio $\zeta = \tau_s^\perp/\tau_s^\parallel$ [48]. The SRTA in graphene on TMD monolayer has been found to attain giant values on the order of $\zeta \sim 10$–100 [16,17], testifying to the important role played by $H_{\rm sv}$. A simple SRTA model has been proposed in Ref. [49], which assumes that the electronic motion of bare quasiparticles is affected by a weak spin-orbit field with a precession axis randomly changing due to scattering events. This framework provides the dependence of ζ on two important dimensionless parameters, $\lambda_{\rm sv}/\lambda$ and τ_0/τ_*, where τ_0 and τ_* are the sample-specific intravalley and intervalley correlation times, respectively [25]. However, the formalism presented there is limited to the weak SOC regime $\lambda_{\rm SOC}\tau_0 \ll 1$ with $\lambda_{\rm SOC} = \max\{|\lambda|, |\lambda_{\rm sv}|\}$, whereas ultraclean samples can display strong SOC on the order of (or larger than) the disorder broadening [11,13,14]. Meanwhile, the development of a *microscopic* approach capable to provide an intuitive, unified description of spin relaxation processes for arbitrary values of $\lambda_{\rm SOC}\tau_0$ and $\lambda_{\rm SOC}\tau_*$ would be highly desirable. Here, we address this problem by means of the single-particle density matrix formalism. We obtain a set of coupled spin Bloch equations governing the spin dynamics in the effective C_{3v} Hamiltonian in the presence of common sources of disorder [Eq. (1)]. The treatment employed here is strictly valid in the semiclassical transport regime of experimental relevance $|\epsilon| \gg \lambda_{\rm SOC}$, where ϵ is the Fermi energy. However, the qualitative features of the spin relaxation regimes predicted in this work are also expected to manifest at low electronic densities. Rich scenarios are shown to emerge, from simple exponentially decaying spin polarization density to fast damped modes, depending on the relative magnitude of the main energy scales of the problem: λ, $\lambda_{\rm sv}$, $1/\tau_0$, and $1/\tau_*$. Finally, we derive analytic expressions for the SRTA ratio ζ in both weak SOC regime (compatible with Ref. [25]) and the strong SOC regime of ultraclean samples ($\lambda_{\rm SOC}\tau_0 \gtrsim \frac{1}{2}$).

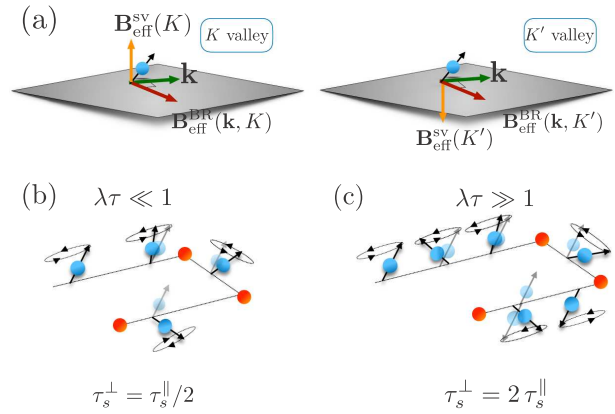

FIG. 1. Spin relaxation in the C_{3v} model. (a) The BR pseudomagnetic field $\mathbf{B}^{\rm BR}_{\rm eff}$ is always orthogonal to the direction of motion $\hat{\mathbf{k}}$ and lies in the plane. On the other hand, the spin-valley pseudomagnetic field $\mathbf{B}^{\rm sv}_{\rm eff}$ (independent of $\mathbf{k}$) has opposite signs in inequivalent valleys: $\mathbf{B}^{\rm sv}_{\rm eff}(\kappa) = -\mathbf{B}^{\rm sv}_{\rm eff}(\bar{\kappa})$, where $\kappa = -\bar{\kappa} = (K, K')$. Spin relaxation regimes: (b) in the pure BR model ($\lambda_{\rm sv} = 0$) spin lifetimes satisfy $\tau_s^\perp = \tau_s^\parallel/2$ for $\lambda\tau \ll 1$; (c) the relation is reversed in the strong SOC limit $\lambda\tau \gg 1$ where $\tau_s^\perp = 2\tau_s^\parallel$. This picture is affected by the spin-valley coupling and intervalley scattering, as discussed in the main text [cf. Eqs. (54)–(59)].

The paper is organized as follows. In Sec. II, we derive the spin Bloch equations governing the spin dynamics in graphene with uniform proximity-induced SOC. In Sec. III, we obtain analytic expressions for the time dependence of the spin polarization in the limiting cases of weak and strong SOC. Section IV discusses the SRTA, putting it in relation with recent theoretical and experimental findings and Sec. V presents our conclusions.

II. FORMALISM: SPIN BLOCH EQUATIONS

The starting point of our approach is the quantum Liouville equation for the single-particle density matrix operator [50–53]

$$\frac{\partial\rho}{\partial t} + \imath\,[\,H_0 + V_{\rm SO} + U, \rho\,] = 0. \tag{5}$$

The interaction U describes uncorrelated disorder

$$U(\mathbf{x}) = U_{\text{intra}}(\mathbf{x}) + U_{\text{inter}}(\mathbf{x}) \tag{6}$$

$$= \sum_{\alpha=0,z} \sum_{\beta=0,x,y,z} [\tau_\alpha \sigma_\beta u_{\alpha\beta}(\mathbf{x})] s_0 \tag{7}$$

$$+ \sum_{\alpha=x,y} \sum_{\beta=0,x,y,z} [\tau_\alpha \sigma_\beta u_{\alpha\beta}(\mathbf{x})] s_0, \tag{8}$$

with Gaussian (white-noise) statistics

$$\langle u_{\alpha\beta}(\mathbf{x}) u_{\alpha'\beta'}(\mathbf{x}')\rangle_{\text{dis}} = u_{\alpha\beta}^2\, \delta_{\alpha\alpha'}\, \delta_{\beta\beta'}\, \delta(\mathbf{x}-\mathbf{x}'). \tag{9}$$

All types of nonmagnetic disorder are included in $U(\mathbf{x})$. Interactions $\propto\sigma_{0,z}$ describe onsite potentials and terms $\propto \sigma_{x,y}$ encode fluctuations in the hopping between neighboring sites (e.g., due to adatoms and ripples) [54]. The terms in the second line [Eq. (8)] mix states on inequivalent valleys, leading to a finite intervalley scattering time. We note that disorders with $\alpha\beta = \{zx, zy, z0, 0z, xz, yx\}$ are not realized in standard conditions (in the absence of external fields) since they break time-reversal symmetry.

In order to derive the general spin Bloch equations governing the spin dynamics for high electronic density, we follow closely the treatment by Culcer and Winkler [51]. The first step is to project Eq. (5) onto plane-wave eigenstates of the unperturbed graphene Hamiltonian, namely,

$$\langle \mathbf{x}|\mathbf{k}\sigma\kappa s\rangle = \frac{1}{\sqrt{2}}\, e^{i\mathbf{k}\cdot\mathbf{x}} |\kappa\rangle \otimes \begin{pmatrix} \kappa\, \sigma\, e^{-\imath\phi_{\mathbf{k}}/2} \\ e^{\imath\phi_{\mathbf{k}}/2} \end{pmatrix} \otimes |s\rangle, \tag{10}$$

where $\mathbf{k}$ is the wave vector (measured from a Dirac point), $\phi_{\mathbf{k}}$ is the wave-vector angle, and $\kappa, \sigma, s = \pm 1$ are indices for valley, sublattice, and spin degrees of freedom, respectively. The free graphene eigenvalues read as $\epsilon_{\mathbf{k}}^{\sigma\kappa s} = \sigma v k$, where $k = |\mathbf{k}|$. ρ is then a matrix of dimension $2^3 = 8$, whose matrix elements are written as $\rho_{\mathbf{k}\mathbf{k}'}^{\alpha\alpha'} = \langle \mathbf{k}'\alpha'|\rho|\mathbf{k}\alpha\rangle$ and $\alpha = \{\sigma, \kappa, s\}$ is shorthand for the set of quantum indices (we use a similar notation for U). V_{SO} has nonzero matrix elements between conduction and valence states leading to interband transitions. However, we focus here on the large Fermi energy regime $\epsilon/\lambda_{\text{SOC}} \gg 1$, where interband coherence effects are strongly suppressed [55]. In what follows, we take $\langle \mathbf{k}'\sigma'|\rho|\mathbf{k}\sigma\rangle = \delta_{\sigma\sigma'}\rho_{\mathbf{k}\mathbf{k}'}$ and fix the Fermi level in the conduction band, dropping the sublattice index ($\sigma = 1$) from the expressions.

Following Ref. [51], we write $\rho_{\mathbf{k}\mathbf{k}'} = f_{\mathbf{k}\mathbf{k}}\delta_{\mathbf{k}\mathbf{k}'} + g_{\mathbf{k}\mathbf{k}'}$, where for $g_{\mathbf{k}\mathbf{k}'}$ it is assumed $\mathbf{k} \neq \mathbf{k}'$. We neglect valley coherence $\langle \kappa'|\rho|\kappa\rangle = \delta_{\kappa\kappa'}$ since typical valley-coherence times are much shorter than the relevant spin-precession and relaxation timescales [56,57]. We have

$$\frac{\partial f_{\mathbf{k}}}{\partial t} + \imath[H_0 + V_{\text{SO}}, f]_{\mathbf{k}\mathbf{k}} = -\imath[U, g]_{\mathbf{k}\mathbf{k}}, \tag{11}$$

$$\frac{\partial g_{\mathbf{k}\mathbf{k}'}}{\partial t} + \imath[H_0 + V_{\text{SO}}, g]_{\mathbf{k}\mathbf{k}'} = -\imath[U, g]_{\mathbf{k}\mathbf{k}'}. \tag{12}$$

We are ultimately interested in the diagonal part $f_{\mathbf{k}\mathbf{k}}$, as the spin observables are defined as

$$\mathbf{S} = \frac{1}{2}\text{Tr}[\rho\cdot\mathbf{s}] = \frac{1}{2}\sum_{\mathbf{k},\kappa} \text{tr}\big[f_{\mathbf{k}\mathbf{k}}^{\kappa}\cdot\mathbf{s}\big] = \frac{1}{2}\sum_{\mathbf{k},\kappa}\mathbf{S}_{\mathbf{k}}^{\kappa}. \tag{13}$$

We hence solve Eq. (12) and substitute the solution into the right-hand side of Eq. (11), which gives the collision integral. After a somewhat lengthy but straightforward calculation, where Eqs. (11) and (12) are expressed in the interaction picture and the evolution operator is expanded to second order in U, one arrives at the following equation for the spin components

$$\partial_t \mathbf{S}_{\mathbf{k}}^{\kappa} + L_{\mathbf{k}}^{\kappa}\mathbf{S}_{\mathbf{k}}^{\kappa} = -\pi \sum_{\mathbf{k}'\kappa'} \delta(\epsilon_{\mathbf{k}} - \epsilon_{\mathbf{k}'}) \big\langle \mathbf{S}_{\mathbf{k}}^{\kappa}\, U_{\mathbf{k}\mathbf{k}'}^{\kappa\kappa'}\, U_{\mathbf{k}'\mathbf{k}}^{\kappa'\kappa} + U_{\mathbf{k}\mathbf{k}'}^{\kappa\kappa'}\, U_{\mathbf{k}'\mathbf{k}}^{\kappa'\kappa}\, \mathbf{S}_{\mathbf{k}}^{\kappa} - 2\, U_{\mathbf{k}\mathbf{k}'}^{\kappa\kappa'}\, \mathbf{S}_{\mathbf{k}'}^{\kappa'}\, U_{\mathbf{k}'\mathbf{k}}^{\kappa'\kappa} \big\rangle_{\text{dis}}, \tag{14}$$

with a Larmor precession term

$$L_{\mathbf{k}}^{\kappa} = 2\begin{pmatrix} 0 & -\kappa\lambda_{\text{sv}} & \lambda\cos\phi_{\mathbf{k}} \\ \kappa\lambda_{\text{sv}} & 0 & \lambda\sin\phi_{\mathbf{k}} \\ -\lambda\cos\phi_{\mathbf{k}} & -\lambda\sin\phi_{\mathbf{k}} & 0 \end{pmatrix}. \tag{15}$$

A comment is in order. Central to our derivation of the quantum kinetic equation is the assumption of Gaussian disorder. Strictly speaking, the latter is equivalent to the first Born approximation [58] and thus it neglects (i) skew scattering (allowed in the C_{3v} model [27], albeit suppressed in the limit $\epsilon/\lambda_{\text{SOC}} \gg 1$ [59]) and (ii) modifications to the energy dependence of the collision integral for realistic (non-Gaussian) disorder with typical momentum scattering time $\tau(\epsilon) \propto \epsilon$ [as opposed to $\tau(\epsilon) \propto \epsilon^{-1}$ for Gaussian disorder] [22]. Importantly, the collision integral [right-hand side of Eq. (14)] retains its form at all orders in the Born series, with U formally replaced by the single-impurity T matrix [24]. For this reason, our final expressions for the spin lifetimes (written in terms of transport scattering times; see below) remain accurate for general types of nonmagnetic static disorder.

Next, we use the quantum kinetic equation (14) to obtain the Bloch equations governing the spin dynamics. First, we separate the collision integral $I[\mathbf{S}_{\mathbf{k}}^{\kappa}]$ into intravalley and intervalley parts, $\kappa' = \{\kappa, \bar{\kappa}\} = \{\kappa, -\kappa\}$. For uncorrelated matrix disorder [Eq. (9)], we find

$$\big\langle \big|U_{\mathbf{k}\mathbf{k}'}^{\kappa\kappa}\big|^2\big\rangle_{\text{dis}} = \sum_{p=\pm}\big[\tilde{u}_p^2 + \big(u_p^2 - \tilde{u}_p^2\big)F_{\mathbf{k}\mathbf{k}'}^{p}\big], \tag{16}$$

$$\big\langle \big|U_{\mathbf{k}\mathbf{k}'}^{\kappa\bar{\kappa}}\big|^2\big\rangle_{\text{dis}} = \sum_{p=\pm}\big[\tilde{w}_p^2 + \big(w_p^2 - \tilde{w}_p^2\big)F_{\mathbf{k}\mathbf{k}'}^{p}\big], \tag{17}$$

where $F_{\mathbf{k}\mathbf{k}'}^{\pm} = \cos^2[(\phi_{\mathbf{k}} \pm \phi_{\mathbf{k}'})/2]$ and

$$u_+^2 = u_{0x}^2 + u_{zx}^2, \quad u_-^2 = u_{00}^2 + u_{z0}^2, \tag{18}$$

$$\tilde{u}_+^2 = u_{0y}^2 + u_{zy}^2, \quad \tilde{u}_-^2 = u_{0z}^2 + u_{zz}^2, \tag{19}$$

$$w_+^2 = u_{xx}^2 + u_{yx}^2, \quad w_-^2 = u_{x0}^2 + u_{y0}^2, \tag{20}$$

$$\tilde{w}_+^2 = u_{xy}^2 + u_{yy}^2, \quad \tilde{w}_-^2 = u_{xz}^2 + u_{yz}^2. \tag{21}$$

Since Gaussian disorder preserves parity $F_{\mathbf{k}\mathbf{k}'}^{\pm} = F_{\mathbf{k}'\mathbf{k}}^{\pm}$, the dynamics of spin polarization density is governed by only three microscopic relaxation rates, which are simple functions of the disorder couplings (see Appendix B). To illustrate the various spin relaxation regimes, it suffices to consider a pair

of couplings leading to a finite intervalley scattering time. Without loss of generality, we choose

$$u \equiv u_- = \sqrt{u_{00}^2 + u_{z0}^2}, \tag{22}$$

$$w \equiv w_- = \sqrt{u_{x0}^2 + u_{y0}^2}. \tag{23}$$

Within the subset of disorder couplings, we can recast the collision integral into the form

$$I^{\rm intra}\big[\mathbf{S}_{\mathbf{k}}^{\kappa}\big] = -2\pi\, u^2 \sum_{\mathbf{k}'} F_{\mathbf{k}\mathbf{k}'}\big(\mathbf{S}_{\mathbf{k}}^{\kappa} - \mathbf{S}_{\mathbf{k}'}^{\kappa}\big)\,\Delta_{\mathbf{k}\mathbf{k}'}, \tag{24}$$

$$I^{\rm inter}\big[\mathbf{S}_{\mathbf{k}}^{\kappa}\big] = -2\pi\, w^2 \sum_{\mathbf{k}'} (1 - F_{\mathbf{k}\mathbf{k}'})\big(\mathbf{S}_{\mathbf{k}}^{\kappa} - \mathbf{S}_{\mathbf{k}'}^{\bar{\kappa}}\big)\,\Delta_{\mathbf{k}\mathbf{k}'}, \tag{25}$$

where $\Delta_{\mathbf{k}\mathbf{k}'} \equiv \delta(\epsilon_{\mathbf{k}} - \epsilon_{\mathbf{k}'})$. To solve the coupled system of 6 equations (3 polarizations $\times$ 2 valleys) [Eq. (14)], we expand $\mathbf{S}_{\mathbf{k}}^{\kappa}$ in cylindric harmonics

$$\mathbf{S}_{\mathbf{k}}^{\kappa} = \sum_{m=-\infty}^{\infty} \mathbf{S}_{k}^{\kappa,m} e^{\imath\, m\, \phi_{\mathbf{k}}}. \tag{26}$$

Substituting Eq. (26) into Eq. (14), and retaining only the lowest-order harmonics $m = 0, \pm 1$, we finally obtain (see Appendix A for details)

$$\partial_t S_x^0 = -\frac{2r^2}{\tau}\big(S_x^0 - \bar{S}_x^0\big) - 2\lambda_{\rm sv} S_y^0 + \lambda \sum_{m=\pm1} S_z^m, \tag{27}$$

$$\partial_t S_y^0 = -\frac{2r^2}{\tau}\big(S_y^0 - \bar{S}_y^0\big) + 2\lambda_{\rm sv} S_x^0 + \imath\lambda \sum_{m=\pm1} m S_z^m, \tag{28}$$

$$\partial_t S_z^0 = -\frac{2r^2}{\tau}\big(S_z^0 - \bar{S}_z^0\big) - \lambda \sum_{m=\pm1} \big(S_x^m + \imath m S_y^m\big), \tag{29}$$

and

$$\partial_t S_x^{\pm1} = \lambda S_z^0 - 2\lambda_{\rm sv} S_y^{\pm1} - h\big(S_x^{\pm1}, \bar{S}_x^{\pm1}\big), \tag{30}$$

$$\partial_t S_y^{\pm1} = \mp\imath\lambda S_z^0 + 2\lambda_{\rm sv} S_x^{\pm1} - h\big(S_y^{\pm1}, \bar{S}_y^{\pm1}\big), \tag{31}$$

$$\partial_t S_z^{\pm1} = -\lambda\big(S_x^0 \mp \imath S_y^0\big) - h\big(S_z^{\pm1}, \bar{S}_z^{\pm1}\big), \tag{32}$$

where

$$h\big(S_i^{\pm1}, \bar{S}_i^{\pm1}\big) = \frac{1}{\tau}\big[(1 + 2r^2) S_i^{\pm1} + r^2 \bar{S}_i^{\pm1}\big], \tag{33}$$

with $(\mathbf{S}_k^{\kappa=\pm1,m})_i \equiv (S_i^m, \bar{S}_i^m)$. We have introduced the ratio of intervalley to intravalley disorder couplings

$$r = w/u \tag{34}$$

and

$$\tau = (u^2 \epsilon / 4v^2)^{-1}, \tag{35}$$

$$\tau_{\rm iv} = \tau/3r^2, \tag{36}$$

the intravalley and intervalley transport scattering times, respectively. The spin Bloch equations [Eqs. (27)–(32)] and the corresponding expressions for the barred component at $\kappa = -1$, obtained by the formal replacement $S \to \bar{S}$ and $\lambda_{\rm sv} \to -\lambda_{\rm sv}$, are the central result of this section. These equations highlight the crucial role played by intervalley scattering ($r > 0$); first term on the right-hand side of Eqs. (27)–(29) for $m = 0$ and last two terms inside brackets in Eq. (33) for $m = \pm 1$.

The spin Bloch equations for the full disorder model have the same structure as Eqs. (27)–(32) with an additional intervalley relaxation rate. The remaining couplings (u_+, w_+, $\tilde{u}_\pm$, and $\tilde{w}_\pm$) are found to (i) renormalize the total τ and $\tau_{\rm iv}$ and (ii) open an additional intervalley channel; see Appendix B for details. For brevity, in what follows we assume $\lambda, \lambda_{\rm sv} > 0$.

III. RESULTS

We are primarily interested in the zeroth harmonics of the various spin components, which according to Eq. (13) completely determine the spin density observables [60]. Below, we derive closed formulas for the time dependence of the spin polarization density in two limiting cases $\lambda \gg \lambda_{\rm sv}$ and $\lambda \ll \lambda_{\rm sv}$.

A. Intravalley scattering only: $w = 0$

The calculations are carried out explicitly for the out-of-plane component $S_z \equiv S_z^0 + \bar{S}_z^0$. The spin Bloch equations are recast in the following form:

$$\begin{pmatrix} \partial_t & \lambda & 0 \\ -4\lambda & \partial_t + \frac{1}{\tau} & 2\lambda_{\rm sv} \\ 0 & -2\lambda_{\rm sv} & \partial_t + \frac{1}{\tau} \end{pmatrix} \begin{pmatrix} S_z \\ y \\ z \end{pmatrix} = \begin{pmatrix} 0 \\ 0 \\ 0 \end{pmatrix}, \tag{37}$$

where we introduced the following admixtures of in-plane spin harmonics:

$$y = \sum_{m=\pm1} \big(S_x^m + \bar{S}_x^m\big) + \imath\, m \,\big(S_y^m + \bar{S}_y^m\big), \tag{38}$$

$$z = \sum_{m=\pm1} \big(S_y^m + \bar{S}_y^m\big) - \imath\, m \,\big(S_x^m + \bar{S}_x^m\big). \tag{39}$$

The eigenfunctions can be written as

$$\begin{pmatrix} S_z(t) \\ y(t) \\ z(t) \end{pmatrix} = \sum_{i=1}^{3} c_i \mathbf{v}_i e^{\omega_i t}, \tag{40}$$

where

ω_i are the the solution of the algebraic equation

$$\omega^3 + \frac{2}{\tau}\omega^2 + \left[4\big(\lambda^2 + \lambda_{\rm sv}^2\big) + \frac{1}{\tau^2}\right]\omega + \frac{4\lambda^2}{\tau} = 0, \tag{41}$$

and $\mathbf{v}_i$ are the corresponding eigenvectors. The coefficients c_i are determined by imposing the Cauchy boundary conditions $S_z^0(t=0) = \frac{1}{2}$, $y(t=0) = z(t=0) = 0$. The analytical solution to Eq. (41) is rather cumbersome. It is more transparent instead to find a solution perturbatively by expanding

$$\omega = \omega^{(0)} + \beta\,\omega^{(1)} + \beta^2 \omega^{(2)} + O(\beta^3), \tag{42}$$

where $\beta = \lambda_{\rm sv}/\lambda$ ($\beta = \lambda/\lambda_{\rm sv}$) representing the case of dominant BR (spin-valley) interaction. We find

$$S_z(t) = \frac{1}{4}\sum_{s=\pm1}\left(1 - \frac{s}{\sqrt{1 - c_z^2}}\right) e^{-\omega_s t} \quad \text{for } \lambda \gg \lambda_{\rm sv}, \tag{43}$$

where $c_z = 4\lambda\tau$ and

$$\omega_s = \frac{\left(1+s\sqrt{1-c_z^2}\right)}{2\tau}\left(1-\frac{\lambda_{\rm sv}^2}{2\lambda^2}\frac{c_z^2}{c_z^2-1+s\sqrt{1-c_z^2}}\right). \tag{44}$$

In the particular case $\lambda_{\rm sv}=0$, we obtain $\omega_s = 1/\tau_s^{\perp}$ with

$$\tau_s^{\perp} = (4\lambda^2\tau)^{-1}, \tag{45}$$

which is the familiar Dyakonov-Perel relation [58]. In this regime, the spin relaxation is governed by motional narrowing, yielding its characteristic dependence $\tau_s \propto \tau^{-1}$ [49,53]. On the other hand, for well-resolved SOC, the electron's spin completes full Larmor precession cycles in-between scattering events, which induces spin-memory loss with a characteristic law $\tau_s \approx 2\tau$ (see Fig. 1 and discussion below) [61–63].

Combining the two limiting cases, we have

$$S_z(t)|_{\lambda\gg\lambda_{\rm sv}} = \frac{1}{2}\begin{cases}\exp\left[-4\lambda^2\tau\, t\left(1-4\lambda_{\rm sv}^2\tau^2\right)\right], & \lambda\tau\ll 1\\ e^{-t/2\tau}\cos\left[2\lambda\, t\left(1+\lambda_{\rm sv}^2/\lambda^2\right)\right], & \lambda\tau\gg 1.\end{cases} \tag{46}$$

The damped oscillatory mode appears when $\lambda \gtrsim 1/2\tau$ similarly to nonchiral 2D electron gases subject to strong BR effect [61–63]. For the in-plane component, we find

$$S_x(t)|_{\lambda\gg\lambda_{\rm sv}} = \frac{1}{2}\begin{cases}\cos(2\lambda_{\rm sv}t)\\ \times\exp\left[-2\lambda^2\tau\, t\left(1-4\lambda_{\rm sv}^2\tau^2\right)\right], & \lambda\tau\ll 1\\ \cos(\lambda t)^2 e^{-\frac{t}{\tau}}, & \lambda\tau\gg 1\end{cases} \tag{47}$$

where the solution in the strong SOC limit includes the higher-order harmonics $m=\pm 2$ [see Eq. (26)]. In samples with dominant spin-valley SOC ($\lambda_{\rm sv}\gg\lambda$), we find instead

$$S_z(t)|_{\lambda_{\rm sv}\gg\lambda} = \frac{1}{2}\exp\left[-\frac{4\lambda^2\tau\, t}{1+4\lambda_{\rm sv}^2\tau^2}\right], \tag{48}$$

which provides the asymptotic behavior

$$S_z(t)|_{\lambda_{\rm sv}\gg\lambda} = \frac{1}{2}\begin{cases}\exp\left[-4\lambda^2\tau\, t\left(1-4\lambda_{\rm sv}^2\tau^2\right)\right], & \lambda_{\rm sv}\tau\ll 1\\ e^{-\frac{t}{\tau}\frac{\lambda^2}{\lambda_{\rm sv}^2}}, & \lambda_{\rm sv}\tau\gg 1.\end{cases} \tag{49}$$

For the in-plane component, we have

$$S_x(t)|_{\lambda_{\rm sv}\gg\lambda} = \frac{1}{2}\begin{cases}\cos(2\lambda_{\rm sv}t)\\ \times\exp\left[-2\lambda^2\tau\, t\left(1-4\lambda_{\rm sv}^2\tau^2\right)\right], & \lambda_{\rm sv}\tau\ll 1\\ \cos\left[2\lambda_{\rm sv}t\left(1+\frac{\lambda^2}{\lambda_{\rm sv}^2}\right)\right]e^{-\frac{t}{2\tau}\frac{\lambda^2}{\lambda_{\rm sv}^2}}, & \lambda_{\rm sv}\tau\gg 1\end{cases} \tag{50}$$

with the transition between overdamped and damped oscillatory modes occurring for $\lambda_{\rm sv}\gtrsim 1/\tau$.

These results deserve some comments. For strong BR interaction ($\lambda_{\rm sv}\ll 1/\tau\ll\lambda$), the second line of Eqs. (46) and (47), the spin polarization density includes an oscillatory component. Note, however, that only in-plane spins experience spin-valley-modulated precession, with small frequency $\omega = 2\lambda_{\rm sv}\ll\lambda$ in this particular regime; see Eq. (47), first line. The lack of spin-valley-driven precession for out-of-plane spins can be understood from simple commutator algebra $\partial_t S_z \propto \imath[H_{\rm sv}, S_z] = 0$. In the limiting case of strong spin-valley interaction ($\lambda\ll 1/\tau\ll\lambda_{\rm sv}$), this reflects in a purely decaying (overdamped) mode for S_z [second line of Eq. (49)] and underdamped behavior for S_x with a large frequency $\omega = 2\lambda_{\rm sv}\gg\lambda$; see second line of (50). As we show in the following section, the spin dynamics in clean samples with long $\tau_{\rm iv}$ display similar behavior (viz. Fig. 2).

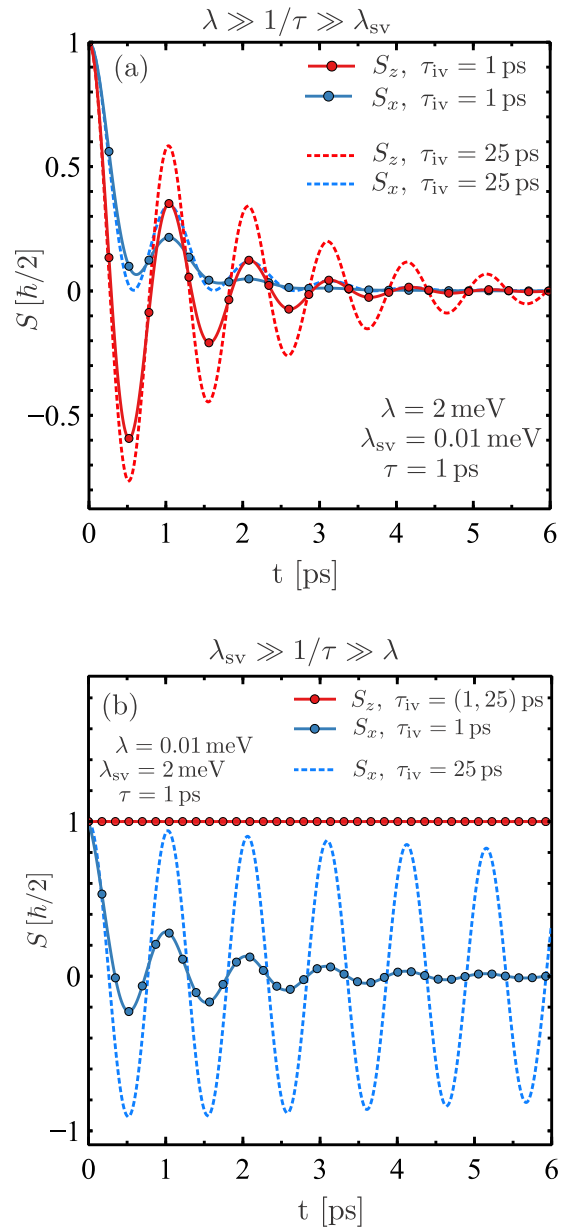

FIG. 2. Spin dynamics for strong proximity-induced SOC ($\lambda_{\rm SOC}\tau\gg 1$) in the presence of intervalley scattering. For dominant BR-type SOC (a), the spin dynamics displays characteristic fast oscillations with lifetime set by the momentum scattering timescale, as discussed in the main text and illustrated in Fig. 1. For dominant spin-valley-type SOC (b) the out-of-plane component is weakly sensitive to the value of $\tau_{\rm iv}$. This is expected to hold in the highly doped regime $\epsilon\gg\lambda_{\rm sv}$, as discussed in the main text. In (a) the traces S_x are calculated including higher-order harmonics up to $m=\pm 2$.

In systems with $\lambda \gg \lambda_{\rm sv}, 1/\tau$, the spin lifetimes are given by $\tau_s^{\parallel} = \tau$ and $\tau_s^{\perp} = 2\tau$. Here, a single scattering event suffices to randomize the electron's spin. The faster decay rate of in-plane spin polarization component indicates the dominant role of $|m| = 2$ contributions in the harmonic expansion (26), yielding a SRTA ratio $\zeta = 2$. For dominant spin-valley interaction ($\lambda_{\rm sv} \gg \lambda$), the spin lifetime is extremely long and, as such, in-plane spins can precess coherently. As pointed out in Ref. [25], this behavior is dramatically changed when intervalley scattering is included in the picture (see below). For weak SOC, namely, $\lambda \ll \lambda_{\rm sv} \ll 1/\tau$ and $\lambda_{\rm sv} \ll \lambda \ll 1/\tau$, the spin dynamics is of the Dyakonov-Perel type, i.e., $\tau_s \propto \tau^{-1}$, as reported in the first lines of Eqs. (46), (47) and (49), (50). In the former case, the spin-valley interaction leads to a correction of order $\propto \lambda_{\rm sv}^2/\lambda^2$ to the well-known Dyakonov-Perel spin relaxation law of BR models [30,49,58]. In the weak SOC regime (for finite λ), the spin lifetimes satisfy the standard ratio $\zeta \simeq 1/2$. On the other hand, the limiting case of vanishingly small BR interaction $\lambda \ll \lambda_{\rm sv} \ll 1/\tau$ is very different in this respect. The valley-Zeeman-like interaction does not couple to electrons' velocity and, at a given valley, its direction is fixed ($\pm\hat{z}$). Thus, in this case, no randomization of the precession axis can occur and the spin relaxation is efficiently suppressed as $\lambda \to 0$. Yet, a small BR interaction is sufficient to relax the spins via motional narrowing, as reported in our equations.

From these results, the SRTA ratio for *intravalley disorder* is readily obtained

$$\zeta|_{\tau_{\rm iv}\to\infty} = \begin{cases} 2, & \lambda\tau \gg \{1, \lambda_{\rm sv}\tau\} \\ 1/2, & \text{all other cases.} \end{cases} \tag{51}$$

In samples with strong BR interaction $\lambda \gg \lambda_{\rm sv}, 1/\tau$, the quantum kinetic theory predicts a SRTA ratio $\zeta = 2$. This difference with respect to the standard Dyakonov-Perel regime, $\zeta = \frac{1}{2}$, stems from the distinct role of the SU(2) gauge field in the two cases $\lambda\tau \ll 1$ and $\lambda\tau \gg 1$. It can be readily verified by inspecting Eq. (15) that the precession period for in-plane and out-of-plane spins must satisfy $T_\perp = T_\parallel/2$ across all regimes. In the spin motional-narrowing limit (random dynamics) mentioned above, with $\lambda\tau \ll 1$, the faster precession of out-of-plane spins reflects in a different step of the random walk $\delta\varphi_\perp = 2\delta\varphi_\parallel$, hence, $\tau_s^\perp = \tau_s^\parallel/2$ [Fig. 1(b)]. On the other hand, for $\lambda\tau \gg 1$, spins relax on the timescale of a single-impurity scattering event. Here, the in-plane spin dynamics is driven by the higher-order harmonics $S_x^{\kappa,\pm 2}$ and the inverse relation is found $\tau_s^\perp = 2\tau_s^\parallel$.

B. Intervalley scattering case: $w \neq 0$

Atomically sharp defects lead to finite intervalley scattering time even in the cleanest samples [11]. Thus, the inclusion of intervalley processes in the collision integral [Eq. (14)] is crucial to understand the spin dynamics in realistic conditions. A similar procedure as outlined in Sec. III A yields the spin Bloch equations

$$\begin{pmatrix} \partial_t & \lambda & 0 \\ -4\lambda & \partial_t + \frac{1}{\tau_+} & 2\lambda_{\rm sv} \\ 0 & -2\lambda_{\rm sv} & \partial_t + \frac{1}{\tau_-} \end{pmatrix} \begin{pmatrix} S_z \\ y \\ z \end{pmatrix} = \begin{pmatrix} 0 \\ 0 \\ 0 \end{pmatrix}, \tag{52}$$

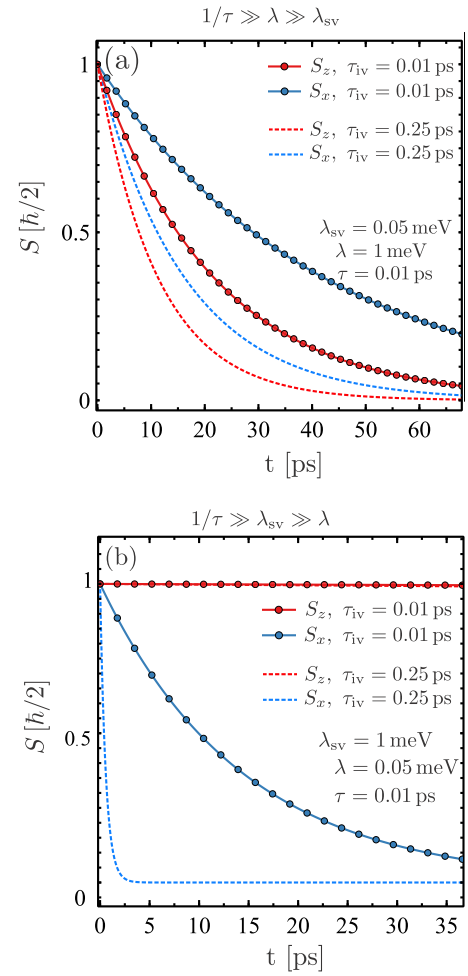

FIG. 3. Spin dynamics for weak proximity-induced SOC ($\lambda_{\rm SOC}\tau \ll 1$) in the presence of intervalley scattering, for $\lambda_{\rm sv} \ll \lambda$ ($\lambda \ll \lambda_{\rm sv}$) [panels (a) and (b), respectively]. In (b), the in-plane spin polarization is more sensitive to the value of $\tau_{\rm iv}$, whereas out-of-plane spins are virtually unaffected by a finite $\tau_{\rm iv}$. This is consistent with the findings in Ref. [25].

with

$$\frac{1}{\tau_\pm} = \frac{1}{\tau} + \frac{1}{3} \times \frac{2 \pm 1}{\tau_{\rm iv}}. \tag{53}$$

We obtain the following asymptotic solutions for the out-of-plane spin polarization density:

$$S_z(t)|_{\lambda \gg \lambda_{\rm sv}} = \frac{1}{2} \begin{cases} \exp\left[-4\lambda^2 \tau_+ t \left(1 - 4\lambda_{\rm sv}^2 \tau_+ \tau_-\right)\right], & \lambda\tau \ll 1 \\ \cos\left[2\lambda\left(1 + \frac{\lambda_{\rm sv}^2}{\lambda^2}\right)t\right] e^{-t/2\tau_+}, & \lambda\tau \gg 1 \end{cases} \tag{54}$$

and

$$S_z(t)|_{\lambda \ll \lambda_{\rm sv}} = \frac{1}{2} \begin{cases} \exp\left[-4\lambda^2 \tau_+ t \left(1 - 4\lambda_{\rm sv}^2 \tau_+ \tau_-\right)\right], & \lambda_{\rm sv}\tau \ll 1 \\ e^{-\frac{t}{\tau_-}\frac{\lambda^2}{\lambda_{\rm sv}^2}}, & \lambda_{\rm sv}\tau \gg 1. \end{cases} \tag{55}$$

Note that as we are interested in the SRTA, in the small SOC cases $\lambda_{\rm SOC}\tau \ll 1$ we also took the limit $\lambda_{\rm SOC}\tau_{\rm iv} \ll 1$, where one can ignore the oscillating factors $\cos(2\lambda_{\rm sv}t)$ reported in

the previous section [Eqs. (47) and (50)]. Considering the in-plane components, we reduce the set of coupled equations [Eqs. (27)–(32)] to only two independent equations coupling $S_x = S_x^0 + \bar{S}_x^0$ and $\tilde{S}_y = S_y^0 - \bar{S}_y^0$,

$$\begin{pmatrix} \partial_t^2 + 2\lambda^2 + \frac{\partial_t}{\tau_+} & 2\lambda_{\rm sv}\left(\partial_t + \frac{1}{\tau_+}\right) \\ -2\lambda_{\rm sv}\left(\partial_t + \frac{1}{\tau_-}\right) & \partial_t^2 + 2\tilde{\lambda}^2 + \frac{\partial_t}{\tau} + \frac{5}{3}\frac{\partial_t}{\tau_{\rm iv}} \end{pmatrix} \begin{pmatrix} S_x \\ \tilde{S}_y \end{pmatrix} = \begin{pmatrix} 0 \\ 0 \end{pmatrix}, \tag{56}$$

where we have defined

$$2\tilde{\lambda}^2 = 2\lambda^2 + \frac{4}{3}\frac{1}{\tau_{\rm iv}}\frac{1}{\tau_-}. \tag{57}$$

Solving Eq. (56) with the usual boundary conditions, i.e., $S_x(t=0) = \frac{1}{2}$ and all the other functions being zero at the initial time, we find

$$S_x(t)|_{\lambda \gg \lambda_{\rm sv}} = \frac{1}{2}\begin{cases} \exp\left[-\left(2\lambda^2\tau_+ + 3\lambda_{\rm sv}^2\tau_{\rm iv}\right)t\right], & \lambda\tau \ll 1 \\ \exp\left[-\left(1/2\tau_+ + 3\lambda_{\rm sv}^2\tau_{\rm iv}\right)t\right] \\ \times \cos(\lambda t)^2, & \lambda\tau \gg 1 \end{cases} \tag{58}$$

and

$$S_x(t)|_{\lambda \ll \lambda_{\rm sv}} = \frac{1}{2}\begin{cases} \exp\left[-\left(2\lambda^2\tau_+ + 3\lambda_{\rm sv}^2\tau_{\rm iv}\right)t\right], & \lambda_{\rm sv}\tau \ll 1 \\ \cos\left(2\lambda_{\rm sv}t\right)e^{-\left(\frac{\lambda^2}{2\lambda_{\rm sv}^2}\frac{1}{\tau} + \frac{2}{3}\frac{1}{\tau_{\rm iv}}\right)t}, & \lambda_{\rm sv}\tau \gg 1. \end{cases} \tag{59}$$

In Figs. 2 and 3, we show representative examples of the spin polarization dynamics in the strong and weak SOC limits, respectively, according to our results.

IV. SPIN RELAXATION TIME ANISOTROPY

The spin Bloch equations (27)–(32), showing a crossover between overdamped (weak SOC) and oscillating damped modes (strong SOC), are the most important result of this paper. We now discuss in more detail how the SRTA evolves from weak interface-induced SOC ($\lambda_{\rm SOC}\tau \ll 1$) to well-resolved SOC ($\lambda_{\rm SOC}\tau \gtrsim 1$). We focus on the asymptotic regimes

$$\zeta = \begin{cases} \frac{1}{2} + \frac{3}{4}\frac{\lambda_{\rm sv}^2}{\lambda^2}\left(1 + \frac{\tau_{\rm iv}}{\tau}\right), & \lambda\tau, \lambda_{\rm sv}\tau \ll 1 \\ 2 + O\left(\lambda_{\rm sv}^2/\lambda^2\right), & \lambda\tau \gg 1 \gg \lambda_{\rm sv}\tau \\ \frac{1}{1+3\frac{\tau_{\rm iv}}{\tau}}\left[\frac{2\lambda_{\rm sv}^2}{\lambda^2} + \frac{3}{2}\frac{\tau_{\rm iv}}{\tau}\right], & \lambda_{\rm sv}\tau \gg 1 \gg \lambda\tau. \end{cases} \tag{60}$$

For the sake of clarity, we note that the first line in the expression for ζ is obtained by considering the first line of Eq. (59) [or equivalently Eq. (58)] together with the first line of Eq. (54) [or Eq. (55)]. The second line of Eq. (60) is obtained using the second lines of Eqs. (58) and (54). Finally, the third line of Eq. (60) is a result of the second lines of Eqs. (59) and (55).

The first important observation concerns the strong BR case with $\lambda\tau \gg 1 \gg \lambda_{\rm sv}\tau$, which can in principle be achieved in clean graphene-based heterostructures, where also the lattice mismatch is sizable enough to produce $\lambda_{\rm sv} \approx 0$. Contrary to the other two presented cases [first and third lines of Eq. (60)], in this limit a direct estimation of $\tau_{\rm iv}/\tau$ or $\lambda_{\rm sv}/\lambda$

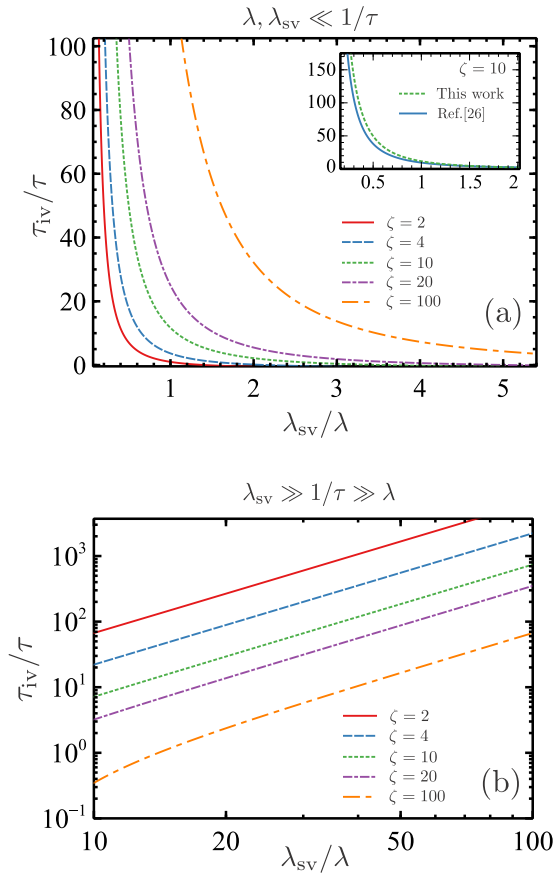

FIG. 4. Traces of fixed SRTA for weak (a) and strong (b) proximity-induced SOC [Eq. (60)]. (a) The inset shows a comparison with the spin white-noise model in Ref. [25] for $\zeta = 10$. (b) Traces of fixed SRTA in the strong SOC regime, Eq. (60), third line. The typical ratio $\tau_{\rm iv}/\tau \sim 25$ [64] is compatible with a broad range of SOCs in the interval $\lambda_{\rm sv}/\lambda = 14$–$80$ depending on the measured SRTA ratio.

from spin precession measurements alone is not possible. Hence, whenever $\zeta \approx 2$ is measured, the extraction of other parameters from spin precession data should be considered unfeasible.

We focus in the following on the two more interesting cases $\lambda\tau, \lambda_{\rm sv}\tau \ll 1$ and $\lambda_{\rm sv}\tau \gg 1 \gg \lambda\tau$. For the weak SOC case [first line of Eq. (60)] we report a visualization of the obtained result in terms of contour lines for fixed ζ [see Fig. 4(a)]. Our results in this limit are in good qualitative agreement with the toy model of fluctuating spins put forward in Ref. [25], i.e.,

$$\zeta = \frac{1}{2} + \frac{\lambda_{\rm sv}^2}{\lambda^2}\frac{\tau_{\rm iv}}{\tau} \quad \text{(Ref. [26])}, \tag{61}$$

$$\zeta = \frac{1}{2} + \frac{1}{4}\frac{\lambda_{\rm sv}^2}{\lambda^2}\left(3 + \frac{\tau_{\rm iv}}{\tau}\right) \quad \text{(this work)}, \tag{62}$$

where, for simplicity, we identified the ratio of intervalley to intravalley correlation time in Ref. [25] with the ratio $\tau_{\rm iv}/\tau$. The inset of Fig. 4(a) shows a detailed comparison for the case $\zeta = 10$. Following the experiment in Ref. [17] ($\zeta = 11$), assuming $\lambda_{\rm sv}/\lambda \sim 0.67$ for graphene/$MoSe_2$ [18], a $\tau_{\rm iv}/\tau = 30$ is obtained, which for $\tau = 0.076$ ps gives $\tau_{\rm iv} = 2.2$ ps (against $\tau_{\rm iv} = 1.7$ ps following Ref. [25]). These estimates (obtained from modeling of spin precession data)

agree qualitatively well with typical relaxation times extracted from magnetotransport measurements [11,64]. We would like to point out that our Eq. (62) [and similarly Eq. (61)] gives a divergent SRTA in the limit of absence of intervalley scattering $\tau_{\rm iv} \to \infty$, at first glance contradicting Eq. (51). The dilemma is solved by noticing that Eq. (62) is strictly valid for $\lambda_{\rm sv}\tau \sim \lambda_{\rm sv}\tau_{\rm iv} \ll 1$. This particular case corresponds to the physical situation where the out-of-plane component of the "SOC field" is randomized on a timescale $\tau_{\rm iv}$ (recall that $H^{\kappa}_{\rm sv} = -H^{\bar\kappa}_{\rm sv}$). This activates a dominant motional-narrowing channel for the in-plane spin component, which strongly impacts the spin dynamics as shown in Fig. 3.

A careful analysis of the crossover to the strong $\lambda_{\rm sv}$ regime allows to conclude that the transition between the motional-narrowing (Dyakonov-Perel) regime $\lambda_{\rm sv}\tau_{\rm iv} \ll 1$ and the fast (oscillating) relaxation regime with $\lambda_{\rm sv}\tau_{\rm iv} \gg 1$ is achieved for $\lambda_{\rm sv}\tau_{\rm iv} \simeq \frac{1}{3}$, assuming $\lambda \ll \lambda_{\rm sv}$. We briefly discuss the experimental conditions for which the strong spin-valley case of Eq. (60) (third line) may be relevant. For instance, in Ref. [12], the authors estimate $\lambda_{\rm sv} = 0.96$ meV $\sim 32\,\lambda$, with $\tau \sim 12$ ps for a graphene/WS_2 heterostructure. Assuming a SRTA ratio $\zeta = 11$ (see above) and using Eq. (61) from Ref. [25] [or, equivalently, first line in Eq. (60)] one would obtain an unphysical result $\tau_{\rm iv}/\tau \simeq 0.01 < 1$. The usage of Eq. (60) in the limit of strong spin-valley coupling then is required. Using this relation, we estimate $\tau_{\rm iv}/\tau \approx 70$, which would suggest a dominant role of intravalley processes in the experiment of Ref. [12].

V. CONCLUSIONS

In this work, we investigated theoretically the spin dynamics in graphene with strong proximity-induced SOC. Starting from the quantum Liouville equation, we derived the effective spin Bloch equations governing the spin dynamics of 2D Dirac fermions subject to "in-plane" (Bychkov-Rashba) and "out-of-plane" (spin-valley) interactions. We discussed in detail the irreversible loss of spin information with origin in intravalley and intervalley scattering processes induced by generic nonmagnetic disorder, obtaining the time dependence of the spin polarization density and associated spin relaxation times. We finally discussed the interesting results for the spin relaxation time anisotropy $\tau_s^{\perp}/\tau_s^{\parallel}$, which is an experimentally accessible figure of merit [48]. The theoretical results reported in Ref. [25] for weak SOC are qualitatively reproduced by our microscopic theory. On the other hand, in ultraclean samples with strong SOC on the order of (or larger than) the disorder-induced quasiparticle broadening, our microscopic theory uncovers a qualitatively different spin relaxation picture. Here, the spin polarization density undergoes fast damped oscillations with spin lifetime set by the timescale of momentum scattering. If Bychkov-Rashba interaction dominates ($\lambda \gg \lambda_{\rm sv}, 1/\tau$), our theory predicts $\tau_s^{\perp}/\tau_s^{\parallel} = 2$. For samples with dominant spin-valley interaction ($\lambda_{\rm sv} \gg \lambda, 1/\tau$), the spin relaxation anisotropy acquires a strong dependence on the relevant intravalley and intervalley scattering times.

We remark that the formalism adopted here is only valid in the highly doped regime of large Fermi energy, where the only role of the "SOC field" is to induce Larmor precession. This picture might break down at low electronic density for graphene with large interface-induced SOC of order 1–10 meV. When the spin texture of the energy bands is well established, momentum is then strongly correlated with the direction of the SOC field, which can favor or inhibit certain matrix elements of the scattering potential U [25]. A possibility to incorporate the SOC at low electronic densities is by adopting the self-consistent quantum diagrammatic formalism for 2D Dirac fermions recently developed in Ref. [58]. We will address this problem in a future publication.

In compliance with EPSRC policy framework on research data, this publication is theoretical work that does not require supporting research data.

ACKNOWLEDGMENTS

We would like to thank R. Raimondi for useful discussions about spin relaxation in two-dimensional electron gases. A.F. gratefully acknowledges the financial support from the Royal Society (U.K.) through a Royal Society University Research Fellowship. M.O. and A.F. acknowledge partial funding from EPSRC (Grant No. EP/N004817/1).

APPENDIX A: DETAILS ON THE DERIVATION OF THE SPIN BLOCH EQUATIONS

The collision integral [Eq. (A1)] is diagonal in valley space $\langle \mathbf{k}\kappa | I | \mathbf{k}'\bar\kappa \rangle = 0$, which was justified in the main text:

$$\partial_t \mathbf{S}^{\kappa}_{\mathbf{k}}\big|_{\rm scatt} = \langle \mathbf{k}\kappa | I | \mathbf{k}\kappa \rangle \equiv I\big[\mathbf{S}^{\kappa}_{\mathbf{k}}\big] \tag{A1}$$

$$= -\pi \sum_{\mathbf{k}'\kappa'} \delta(\epsilon_{\mathbf{k}} - \epsilon_{\mathbf{k}'}) \big\langle \mathbf{S}^{\kappa}_{\mathbf{k}}\, U^{\kappa\kappa'}_{\mathbf{k}\mathbf{k}'}\, U^{\kappa'\kappa}_{\mathbf{k}'\mathbf{k}} + U^{\kappa\kappa'}_{\mathbf{k}\mathbf{k}'}\, U^{\kappa'\kappa}_{\mathbf{k}'\mathbf{k}}\, \mathbf{S}^{\kappa}_{\mathbf{k}} - 2\, U^{\kappa\kappa'}_{\mathbf{k}\mathbf{k}'}\, \mathbf{S}^{\kappa'}_{\mathbf{k}'}\, U^{\kappa'\kappa}_{\mathbf{k}'\mathbf{k}} \big\rangle_{\rm dis}. \tag{A2}$$

Intervalley processes are still taken into account *internally* to the collision integral, i.e., by considering transitions of the type $K \to K' \to K$ where electrons initially at $K(K')$ are scattered at $K'(K)$ and then scattered back to $K(K')$. Inserting the disorder correlator

$$\big\langle \big| U^{\kappa\kappa'}_{\mathbf{k}\mathbf{k}'} \big|^2 \big\rangle_{\rm dis} = u^2\, \delta_{\kappa\kappa'} \cos^2\theta + w^2 \delta_{\kappa\bar\kappa'} \sin^2\theta, \tag{A3}$$

$$\theta \equiv \frac{\phi_{\mathbf{k}'} - \phi_{\mathbf{k}}}{2} \tag{A4}$$

into Eq. (A1) gives Eqs. (24) and (25) in the main text. Using the notation in the main text and the relation

$$2\pi\, u^2 \int_0^{\infty} \frac{dk'}{2\pi} k' \delta(\epsilon_{\mathbf{k}} - \epsilon_{\mathbf{k}'}) = \frac{u^2 \epsilon}{v^2} \equiv \frac{4}{\tau}, \tag{A5}$$

where the intravalley transport time τ has been defined, yields, after simple algebra

$$I^{\rm intra} = -\frac{4}{\tau}\sum_m e^{\imath\, m\phi_{\mathbf{k}}}\int_0^{2\pi}\frac{d\phi_{\mathbf{k}'}}{2\pi}\cos^2\left(\frac{\phi_{\mathbf{k}}-\phi_{\mathbf{k}'}}{2}\right) \times\left[1-e^{-\imath\, 2m\left(\frac{\phi_{\mathbf{k}}-\phi_{\mathbf{k}'}}{2}\right)}\right]S_i^m \tag{A6}$$

$$= -\frac{4}{\tau}\sum_m e^{\imath\, m\,\phi_{\mathbf{k}}}S_i^m\int_0^{2\pi}\frac{d\theta}{2\pi}\cos^2\theta(1-\cos 2\,m\,\theta) \tag{A7}$$

$$\equiv -\sum_{m\neq 0} e^{\imath\, m\,\phi_{\mathbf{k}}}\frac{S_i^m}{\tau_m^A}, \tag{A8}$$

with

$$\frac{1}{\tau_m^A} = \frac{4}{\tau}\int_0^{2\pi}\frac{d\theta}{2\pi}\cos^2\theta[1-\cos(2\,m\,\theta)]. \tag{A9}$$

The intervalley part reads as

$$I^{\rm inter} = -\frac{4}{\tau}r^2\left\{\sum_m e^{\imath\, m\,\phi_{\mathbf{k}}}\int_0^{2\pi}\frac{d\phi_{\mathbf{k}'}}{2\pi}\sin^2\left(\frac{\phi_{\mathbf{k}}-\phi_{\mathbf{k}'}}{2}\right) \times\left[S_i^m-\bar{S}_i^m e^{-\imath\, 2m\left(\frac{\phi_{\mathbf{k}}-\phi_{\mathbf{k}'}}{2}\right)}\right]\right\} \tag{A10}$$

$$= -\frac{4}{\tau}r^2\left(\sum_m e^{\imath\, m\,\phi_{\mathbf{k}}}\frac{S_i^m}{2}-\bar{S}_i^m\int_0^{2\pi}\frac{d\theta}{2\pi}\sin^2\theta\,\cos 2\,m\,\theta\right) \tag{A11}$$

$$= -r^2\sum_m e^{\imath\, m\,\phi_{\mathbf{k}}}\left(\frac{2S_i^m}{\tau}-\frac{\bar{S}_i^m}{\tau_m^B}\right), \tag{A12}$$

with

$$\frac{1}{\tau_m^B} = \frac{4}{\tau}\int_0^{2\pi}\frac{d\theta}{2\pi}\sin^2\theta\cos(2\,m\,\theta). \tag{A13}$$

It is instructive to consider the system *without* SOC, for which the various harmonics are decoupled

$$\partial_t S_i^m = -\left(\frac{1}{\tau_m^A}+\frac{2r^2}{\tau}\right)S_i^m+\frac{r^2}{\tau_m^B}\bar{S}_i^m, \tag{A14}$$

$$\partial_t \bar{S}_i^m = -\left(\frac{1}{\tau_m^A}+\frac{2r^2}{\tau}\right)\bar{S}_i^m+\frac{r^2}{\tau_m^B}S_i^m, \tag{A15}$$

and the corresponding expression at K', obtainable by $S\to\bar{S}$. Solving these equations, we obtain

$$\begin{pmatrix}S_i^m(t)\\ \bar{S}_i^m(t)\end{pmatrix} = e^{-\left(\frac{1}{\tau_m^A}+2r^2\frac{t}{\tau}\right)}\begin{pmatrix}\cosh\left(t\frac{r^2}{\tau_m^B}\right) & \sinh\left(t\frac{r^2}{\tau_m^B}\right)\\ \sinh\left(t\frac{r^2}{\tau_m^B}\right) & \cosh\left(t\frac{r^2}{\tau_m^B}\right)\end{pmatrix} \times\begin{pmatrix}S_i^m(0)\\ \bar{S}_i^m(0)\end{pmatrix}. \tag{A16}$$

For $m=0$, we have $\tau_0^A\to\infty$ and $\tau_0^B\to\tau/2$, so that the solution for the total spin polarization is found as $S_i(t) = S_i^0(t)+\bar{S}_i^0(t) = S_i(t=0)$, which is simply a statement of spin conservation. Note that the uniform oscillation (zeroth harmonic) of the Fermi surface is associated with the charge density. Restoring SOC, and defining $\tau_{\pm1}^A = \tau = -\tau_{\pm1}^B$ we find Eqs. (27)–(32) of the main text for the harmonics $m = 0,\pm1$.

APPENDIX B: GENERAL NONMAGNETIC DISORDER

The correlator for generic nonmagnetic disorder reads as

$$\left\langle\left|U_{\mathbf{kk}'}^{\kappa\kappa'}\right|^2\right\rangle_{\rm dis} = \sum_{p=\pm}\left[\left(u_p^2\,\delta_{\kappa\kappa'}+\tilde{w}_p^2\delta_{\kappa\bar{\kappa}'}\right)\cos^2\theta_p + \left(w_p^2\delta_{\kappa\bar{\kappa}'}+\tilde{u}_p^2\,\delta_{\kappa\kappa'}\right)\sin^2\theta_p\right], \tag{B1}$$

$$\theta_\pm \equiv \frac{\phi_{\mathbf{k}'}\pm\phi_{\mathbf{k}}}{2}. \tag{B2}$$

It is convenient to define the relaxation rates [see main text, Eqs. (18)–(21)]

$$\frac{1}{\tau_u^p} = \frac{u_p^2\epsilon}{4v^2},\quad \frac{1}{\tau_{\tilde{u}}^p} = \frac{\tilde{u}_p^2\epsilon}{4v^2},\quad \frac{1}{\tau_w^p} = \frac{w_p^2\epsilon}{4v^2},\quad \frac{1}{\tau_{\tilde{w}}^p} = \frac{\tilde{w}_p^2\epsilon}{4v^2}. \tag{B3}$$

Following the same steps as in Appendix A, we find

$$I^{\rm intra} = -4\sum_m e^{\imath\, m\phi_{\mathbf{k}}}\int_0^{2\pi}\frac{d\phi_{\mathbf{k}'}}{2\pi}\left(\frac{1}{\tau_u^-}\cos^2\theta_-+\frac{1}{\tau_u^+}\cos^2\theta_+ + \frac{1}{\tau_{\tilde{u}}^-}\sin^2\theta_-+\frac{1}{\tau_{\tilde{u}}^-}\sin^2\theta_+\right)(1-e^{-\imath\, 2m\,\theta_-})S_i^m \tag{B4}$$

$$= -\sum_{m\neq 0}e^{\imath\, m\,\phi_{\mathbf{k}}}\frac{S_i^m}{\tau_{KK}}+\left(\frac{1}{\tau_u^+}-\frac{1}{\tau_{\tilde{u}}^+}\right) \times\left(e^{5\imath\phi_{\mathbf{k}}}S_i^1+e^{-5\imath\phi_{\mathbf{k}}}S_i^{-1}\right), \tag{B5}$$

where

$$\frac{1}{\tau_{KK}} = \frac{1}{\tau_u^-}+\frac{3}{\tau_{\tilde{u}}^-}+\frac{2}{\tau_u^+}+\frac{2}{\tau_{\tilde{u}}^+}. \tag{B6}$$

The intervalley part of the collision integral reads as

$$I^{\rm inter} = -4\sum_m e^{\imath\, m\phi_{\mathbf{k}}}\int_0^{2\pi}\frac{d\phi_{\mathbf{k}'}}{2\pi}\left(\frac{1}{\tau_{\tilde{w}}^-}\cos^2\theta_-+\frac{1}{\tau_{\tilde{w}}^+}\cos^2\theta_+ + \frac{1}{\tau_w^-}\sin^2\theta_-+\frac{1}{\tau_w^+}\sin^2\theta_+\right)\left(S_i^m-\bar{S}_i^m e^{-\imath\, 2m\,\theta_-}\right) \tag{B7}$$

$$= -\sum_m e^{\imath\, m\,\phi_{\mathbf{k}}}\left(\frac{S_i^m}{\tau_{KK'}}+\frac{\bar{S}_i^m}{\tau_m^{\rm iv}}\right)-\left(\frac{1}{\tau_w^+}-\frac{1}{\tau_{\tilde{w}}^+}\right) \times\left(e^{-3\imath\phi_{\mathbf{k}}}S_i^1+e^{3\imath\phi_{\mathbf{k}}}S_i^{-1}\right), \tag{B8}$$

where

$$\frac{1}{\tau_{KK'}} = 2\left(\frac{1}{\tau_w^-}+\frac{1}{\tau_{\tilde{w}}^-}+\frac{1}{\tau_w^+}+\frac{1}{\tau_{\tilde{w}}^+}\right),\quad \frac{1}{\tau_0^{\rm iv}} = \frac{1}{\tau_{KK'}},\quad \frac{1}{\tau_{\pm1}^{\rm iv}} = \frac{1}{\tau_w^-}-\frac{1}{\tau_{\tilde{w}}^-}. \tag{B9}$$

The general Bloch equations are thus obtained from Eqs. (27)–(32) in the main text via the following mapping:

$$\frac{2r^2}{\tau}\to\frac{1}{\tau_{KK'}},\qquad h(S_i^\pm,\bar{S}_i^\pm)\to\left(\frac{1}{\tau_{KK}}+\frac{1}{\tau_{KK'}}\right)S_i^{\pm1} + \left(\frac{1}{\tau_w^-}-\frac{1}{\tau_{\tilde{w}}^-}\right)\bar{S}_i^{\pm1}. \tag{B10}$$

[1] A. Geim and I. Grigorieva, Nature (London) **499**, 419 (2013).
[2] R. Mas-Ballesté, C. Gomez-Navarro, J. Gomez-Herrero, and F. Zamora, Nanoscale **3**, 20 (2011).
[3] S. Z. Butler *et al.*, ACS Nano **7**, 2898 (2013).
[4] Y. Zhang, A. Rubio, and G. Le Lay, J. Phys. D: Appl. Phys. **50**, 053004 (2017).
[5] N. Zibouche, P. Philipsen, A. Kuc, and T. Heine, Phys. Rev. B **90**, 125440 (2014).
[6] A. Ferreira, T. G. Rappoport, M. A. Cazalilla, and A. H. Castro Neto, Phys. Rev. Lett. **112**, 066601 (2014).
[7] A. Soumyanarayanan, N. Reyren, A. Fert, and C. Panagopoulos, Nature (London) **539**, 509 (2016).
[8] J. H. Garcia, M. Vila, A. W. Cummings, and S. Roche, Chem. Soc. Rev. **47**, 3359 (2018).
[9] A. Avsar, J. Y. Tan, T. Taychatanapat, J. Balakrishnan, G. K. W. Koon, Y. Yeo, J. Lahiri, A. Carvalho, A. S. Rodin, E. C. T. O' Farrell, G. Eda, A. H. Castro Neto, and B. Özyilmaz, Nat. Commun. **5**, 4875 (2014).
[10] Z. Wang, D. K. Ki, H. Chen, H. Berger, A. H. MacDonald, and A. F. Morpurgo, Nat. Commun. **6**, 8339 (2015).
[11] Z. Wang, D. K. Ki, J. Y. Khoo, D. Mauro, H. Berger, L. S. Levitov, and A. F. Morpurgo, Phys. Rev. X **6**, 041020 (2016).
[12] B. Yang, M. F. Tu, J. Kim, Y. Wu, H. Wang, J. Alicea, R. Wu, M. Bockrath, and J. Shi, 2D Mater. **3**, 031012 (2016).
[13] T. Volkl, T. Rockinger, M. Drienovsky, K. Watanabe, T. Taniguchi, D. Weiss, and J. Eroms, Phys. Rev. B **96**, 125405 (2017).
[14] S. Zihlmann, A. W. Cummings, J. H. Garcia, M. Kedves, K. Watanabe, T. Taniguchi, C. Schonenberger, and P. Makk, Phys. Rev. B **97**, 075434 (2018).
[15] T. Wakamura, F. Reale, P. Palczynski, S. Gueron, C. Mattevi, and H. Bouchiat, Phys. Rev. Lett. **120**, 106802 (2018).
[16] L. A. Benítez, J. F. Sierra, W. Savero Torres, A. Arrighi, F. Bonell, M. V. Costache, and S. O. Valenzuela, Nat. Phys. **14**, 303 (2017).
[17] T. S. Ghiasi, J. Ingla-Aynes, A. A. Kaverzin, and B. J. Van Wees, Nano Lett. **17**, 7528 (2017).
[18] M. Gmitra, D. Kochan, P. Hogl, and J. Fabian, Phys. Rev. B **93**, 155104 (2016).
[19] A. M. Alsharari, M. M. Asmar, and Sergio E. Ulloa, Phys. Rev. B **94**, 241106(R) (2016).
[20] Y. A. Bychkov and E. I. Rashba, ZhETF Pis'ma Redaktsiiu **39**, 66 (1984) [JETP Lett. **39**, 78 (1984)].
[21] S. Singh, A. M. Alsharari, S. E. Ulloa, and A. H. Romero, arXiv:1806.11469.
[22] A. Pachoud, A. Ferreira, B. Ozyilmaz, and A. H. CastroNeto, Phys. Rev. B **90**, 035444 (2014).
[23] A. A. Stabile, A. Ferreira, J. Li, N. M. R. Peres, and J. Zhu, Phys. Rev. B **92**, 121411(R) (2015).
[24] C. Huang, Y. D. Chong, and Miguel A. Cazalilla, Phys. Rev. B **94**, 085414 (2016).
[25] A. W. Cummings, J. H. Garcia, J. Fabian, and S. Roche, Phys. Rev. Lett. **119**, 206601 (2017).
[26] M. Offidani, M. Milletari, R. Raimondi, and A. Ferreira, Phys. Rev. Lett. **119**, 196801 (2017).
[27] M. Milletari, M. Offidani, A. Ferreira, and R. Raimondi, Phys. Rev. Lett. **119**, 246801 (2017).
[28] J. H. Garcia, A. Cummings, and S. Roche, ACS Nano Lett. **17**, 5078 (2017).
[29] V. K. Dugaev, E. Ya. Sherman, and J. Barnaś, Phys. Rev. B **83**, 085306 (2011).
[30] P. Zhang and M. W. Wu, New J. Phys. **14**, 033015 (2012).
[31] D. V. Fedorov, M. Gradhand, S. Ostanin, I. V. Maznichenko, A. Ernst, J. Fabian, and I. Mertig, Phys. Rev. Lett. **110**, 156602 (2013).
[32] D. V. Tuan, F. Ortmann, D. Soriano, S. O. Valenzuela, and S. Roche, Nat. Phys. **10**, 857 (2014).
[33] I. M. Vicent, H. Ochoa, and F. Guinea, Phys. Rev. B **95**, 195402 (2017).
[34] The states are expressed in the basis $(KA\uparrow, KAg\downarrow, KB\uparrow, KB\downarrow, K'B\uparrow, K'B\downarrow, K'A\uparrow, K'A\downarrow)$, where $A(B)$ labels the sublattice, $K(K')$ denotes the valley, and $\uparrow, \downarrow$ are spin projections.
[35] L. Bir and G. E. Pikus, *Symmetry and Strain Induced Effects in Semiconductors* (Wiley, New York, 1974).
[36] R. Winkler, *Spin-Orbit Coupling Effects in Two-Dimensional Electron and Hole Systems* (Springer, Berlin, 2003).
[37] D. Kochan, S. Irmer, and J. Fabian, Phys. Rev. B **95**, 165415 (2017).
[38] V. T. Phong, N. R. Walet, and F. Guinea, 2D Mater. **5**, 014004 (2017).
[39] T. P. Cysne, A. Ferreira, and T. G. Rappoport, Phys. Rev. B **98**, 045407 (2018).
[40] J. W. McClure and Y. Yafet, Proceedings of the Fifth Conference on Carbon **1**, 22 (1962).
[41] J. Jung, Z. Qiao, Q. Niu, and A. H. MacDonald, Nano Lett. **12**, 2936 (2012).
[42] Terms proportional to σ_z have vanishing expectation value with respect to unperturbed (pristine graphene) states, and thus play a secondary role in the high electronic density regime of interest in this work.
[43] H. Min, J. E. Hill, N. A. Sinitsyn, B. R. Sahu, L. Kleinman, and A. H. MacDonald, Phys. Rev. B **74**, 165310 (2006).
[44] D. Huertas-Hernando, F. Guinea, and A. Brataas, Phys. Rev. B **74**, 155426 (2006).
[45] C. L. Kane and E. J. Mele, Phys. Rev. Lett. **95**, 226801 (2005).
[46] X. Xu, W. Yao, D. Xiao, and T. F. Heinz, Nat. Phys. **10**, 343 (2014).
[47] Z. Y. Zhu, Y. C. Cheng, and U. Schwingenschlogl, Phys. Rev. B **84**, 153402 (2011).
[48] B. Raes, J. E. Scheerder, M. V. Costache, F. Bonell, J. F. Sierra, J. Cuppens, J. Van de Vondel, and S. O. Valenzuela, Nat. Commun. **7**, 11444 (2016).
[49] J. Fabian, A. Matos-Abiage, C. Ertler, P. Stano, and I. Zutic, Acta Phys. Slovaca **4**, 565 (2007).
[50] S. A. Tarasenko, JETP Lett. **84**, 199 (2006).
[51] D. Culcer and R. Winkler, Phys. Rev. B **76**, 245322 (2007); **78**, 235417 (2008).
[52] V. K. Dugaev, E. Ya. Sherman, V. I. Ivanov, and J. Barnaś, Phys. Rev. B **80**, 081301(R) (2009).
[53] M. W. Wu, J. H. Jiang, and M. Q. Weng, Phys. Rep. **493**, 61 (2010).
[54] P. M. Ostrovsky, I. V. Gornyi, and A. D. Mirlin, Phys. Rev. B **74**, 235443 (2006).
[55] Since the spin-valley interaction is proportional to the identity matrix in sublattice space σ_0, it cannot mediate interband transitions. Thus, strictly speaking, it suffices to consider $\epsilon/|\lambda| \gg 1$ to neglect interband effects.

[56] Valley-coherent states have been created and detected, e.g., in WSe_2 by optical methods, with valley-coherence time estimated as $\tau_v = 100$ fs at $T = 10$ K [57]. Such timescales are irrelevant for typical Hanle spin precession measurements.

[57] K. Hao, G. Moody, F. Wu, C. Kavir Dass, L. Xu, C. H. Chen, L. Sun, M. Y. Li, L. J. Li, A. H. MacDonald, and X. Li, Nat. Phys. **12**, 677 (2016).

[58] M. Offidani, R. Raimondi, and A. Ferreira, MDPI Condens. Matter **3**, 18 (2018).

[59] M. Offidani and A. Ferreira, Phys. Rev. Lett. **121**, 126802 (2018).

[60] Harmonics with $m = \pm 1$ contain information about spin currents, which couple to the spin density in Eqs. (27)–(32) via the BR interaction

[61] V. N. Gridnev, JETP Lett. **74**, 380 (2001).

[62] P. Schwab, M. Dzierzawa, C. Gorini, and R. Raimondi, Phys. Rev. B **74**, 155316 (2006).

[63] X. Liu, X. J. Liu, and J. Sinova, Phys. Rev. B **84**, 035318 (2011).

[64] F. V. Tikhonenko, D. W. Horsell, R. V. Gorbachev, and A. K. Savchenko, Phys. Rev. Lett. **100**, 056802 (2008).